CHEMIJA. 2013. Vol. 24. No. 1. P. 20–29

EIS study of initial stages of magnetron-sputtered thin-film Mg-25Al-Zn alloy corrosion in ammonium borate solution

L. Staišiūnas,

A. Grigucevičienė,

P. Miečinskas,

D. Bražinskienė,

S. J. Asadauskas,

K. Leinartas*

Institute of Chemistry,
Centre of Physical Sciences
and Technology,
A. Goštauto 9,
LT-01108 Vilnius,
Lithuania

The ~1 μm thick films of Mg-25Al-Zn alloy (at.%: Al – ~25, Zn – 0.5–1.0 and Mg – in balance) were formed on glass substrates by the direct current (DC) magnetron-sputtering technique. Electrochemical impedance spectroscopy (EIS) was used to study the short-term corrosion behavior of as-deposited Mg-25Al-Zn alloy films in ammonium borate solution. As determined, corrosion of alloys was considerably influenced by the microstructure of coatings and by the thickness and electrical resistance of the oxide layer, which developed at the electrode / solution interface. Alloys characterized by the finest grain size and the lesser content of β-phase were more corrosion-resistant. The initial thickness of the oxide layer depended on the alloy formation temperature: it varied from ~5 nm at 10 °C and 40 °C to ~15–20 nm at 150 °C. The EIS method was also used for study of oil-coated Mg-25Al-Zn electrodes. Corrosion behavior of Mg-25Al-Zn alloys coated with a ~5 μm thick film of paraffin mineral oil was very similar. At the same time, it could be noted that paraffin mineral oil suppressed the impact of β-phase. Thickness of the oxide layer decreased during exposure in borate solution. The observed increase in corrosion resistance was attributed to enrichment of the oxide layer with aluminum oxide.

Key words: magnesium alloy, thin film, corrosion, electrochemical impedance spectroscopy, paraffin mineral oil

INTRODUCTION

Pure Mg, characterized by relatively low yield stress, elongation and modulus, is the lightest of known constructing metals (ρ ~1.74 g/cm^3) and has the best stiffness / weight ratio. However, Mg is chemically very active both in air and most aqueous systems. Usually, chemical and mechanical performance of Mg is effectively improved by alloying it with other metals. Currently the most widely used Mg alloys are those with additives of Al, Zn and Mn, such as AZ31, AZ91, and AM50. Rare Earth metals are used for those Mg alloys, which are critically important in aerospace and military sectors. However, it should be noted that alloying of Mg also could produce some detrimental effects, e. g., susceptibility to contact corrosion or predisposition to hot cracking. Due to their outstanding mechanical and physical properties (superb castability, lightweight, stiffness, and high damping capability), Mg-based alloys are considered as very promising materials in automotive and aircraft industries, computer engineering and portable electronics [1–5]. In the automotive industry, the most immediate Mg alloy utilization includes several applications like steering wheel, dashboard mounting bracket, gearbox housing and chassis. Modern requirements of fuel economy emphasized the need for weight reduction in the transportation sector and intensified the search for the most suitable combinations of construction materials.

* Corresponding author. E-mail: leinart@ktl.mii.lt

In recent years, the interest in Mg alloys as biomaterial was ignited, in order to replace the widely used Ti, stainless steels or Co-Cr-based alloys. Mg alloys are appreciated as potentially suitable for bone implants and stent fabrications due to their inherent biocompatibility and adequate mechanical properties, including fracture toughness higher than that of ceramics [6–9]. Biodegradability of Mg alloys, as opposed to traditionally used metals, also presents a major advantage, which offers the possibility of better physiological repair with minimal inflammatory response.

As mentioned above, applications of Mg alloys, especially in technical environment, are severely hindered by poor resistance to corrosion. A very negative standard potential value of Mg/Mg^{2+} (~–2.36 V), which means high susceptibility to galvanic corrosion, also impedes practical use of Mg-based alloys. The main reason for the poor Mg corrosion resistance is a low protective ability and instability of its surface hydroxide layer, which spontaneously forms both in air and aqueous solutions.

Various techniques have been used to improve the bulk or surface passivity of Mg alloys: anodic oxidation, electroplating, physical vapour evaporation, etc. Nevertheless, more effective methods are still in demand. Modern Mg processing methods include formation of supersaturated single-phase and amorphous thin films, surface modification through laser melting, ion implantation, micro-alloying, etc. [6, 10–13]. As known, corrosion resistance of alloys directly correlates with an increase in the concentration of the alloying element or its oxide in the passive film. Refinement of the surface microstructure also plays a significant role in improvement of corrosion properties of alloys [9, 14–19]. Refinement of the microstructure reduces defects of casting such as porosity, shrinkage and hot tearing tendency, enhances creep properties [16, 17]. Formations of fine-grained Mg-based alloys have been the subject of considerable interest in recent years. The application of PVD, CVD, "sol-gel" techniques for formation of fine-grained layers considerably stimulated the development efforts. One of the main requirements for modified coating is the retention of similar properties as well as the assurance of good adhesion between the formed film and substrate. A promising way to ensure these requirements is formation of functionally / compositionally-graded materials. The upper layer of such graded films has to be more corrosion-resistant than the underlying substrate.

When used in technical environment, the surfaces of Mg alloys can be routinely exposed not only to air, light, humidity or dust, but also to oily liquids, such as lubricants, food, or airborne mist. Oils and lubricants play a significant role in performance of industrial and automotive equipment [20–23]. In addition to separating moving surfaces, lubricants remove contaminants, neutralize corrosive acids, protect surfaces from wear, and dissipate heat. Lubricants are often used when urgent action is needed to stop the surface from corroding.

In this work a short-term corrosion of as-deposited and oil-coated magnetron-sputtered Mg-25Al-Zn alloys in ammonium borate solution was studied. The influence of paraffin mineral oil layer on the corrosion behaviour of Mg-25Al-Zn alloy was evaluated in comparison to oil-free counterparts. A thin layer of the studied Mg-25Al-Zn alloy can be used as an intermediate or outer part of the protective metal film. It is expected that due to high Al content the studied alloy would be sufficiently passive. The understanding of initial stages of Mg alloy corrosion is very important for predicting its long-term performance. Corrosion behaviour of magnetron-sputtered Mg-25Al-Zn alloys in electrolytes and, especially, under oil layers is not well understood. The aim of this study is to evaluate the influence of the coating microstructure on the corrosion mechanism in an attempt to construct a thin film of Mg alloys with improved corrosion resistance. General understanding of the oil film influence on the corrosion behaviour of Mg thin film alloys can also be useful in construction of new triboengineered surfaces.

EXPERIMENTAL

A magnetron-sputtering device Univex 350 (Leybold Vacuum GmbH, Germany) was used for deposition of Mg-Al-Zn alloys. The device is equipped with two DC and one RF (radio frequency) confocal magnetrons. Before deposition the sputtering chamber was evacuated to the base pressure of $(1.2–1.4) \times 10^{-6}$ mBar and then filled with high purity Ar, which pressure was maintained at $\sim 1.8 \times 10^{-3}$ mBar. The targets of 50 mm in diameter were prepared from AZ31 (Mg-3Al-1Zn alloy) and Al (purity 99.999%) produced by Alfa Aesar GmbH (Germany). The Mg-25Al-Zn alloys were deposited in the DC mode by simultaneous sputtering of both targets on glass substrates (discs 15 mm in diameter) heated to 10, 40, 80 and 150 °C by the integrated infrared heater. The empirically chosen sputtering power was kept at (100–120) W for AZ31 and ~75 W for Al. To ensure a uniform coating distribution, substrates were rotated at 18 rpm. In all cases the thickness of deposited coatings was ca. 1 μm. In all cases, deposited coatings were subjected to routine procedures of composition and structure control by a microprobe of a scanning electron microscope (SEM) EVO-50 EP (Carl Zeiss SMT AG, Germany) and a D8 Advance diffractometer (Bruker AXS, Germany), respectively. The alloys contained ~25 at.% of Al and minor amounts of Zn (0.5–1.0 at.%), which originated from the AZ31 target. According to X-ray diffraction (XRD) measurements, crystallites of deposited Mg-25Al-Zn alloys present prevailing orientation in [103] crystallographic direction. A substitutional solid solution of Al in magnesium hexagonal close-packed (*hcp*) lattice (α-phase or α-Mg matrix) was formed. The presence of a considerable amount of intermetallic compound $Mg_{17}Al_{12}$ (β-phase) was also determined for alloys formed at 80 and 150 °C: ~85 and ~80 wt.%, respectively. This type of microstructure, consisting of α-Mg matrix with the β-phase

distributed along α-grains boundaries, is typical for Al-containing Mg alloys and is consistent with the literature [2, 3, 24, 25]. The β-phase did not precipitate in alloys formed at 10 and 40 °C. The surface morphology and grain sizes of as-deposited Mg-25Al-Zn alloys were evaluated by an Atomic Force Microscopy (AFM) device Bioscope II (VEECO Instr., USA). The mean grain size of coatings deposited at 10, 40, 80 and 150 °C was ~12, ~50, ~120 and ~200 nm, respectively [26]. The roughness factors (ratio of AFM-measured and geometrical area) of all deposited coatings were very close: 1.05–1.08.

EIS measurements were carried out using a Potentiostat / Galvanostat / Frequency response analyzer (P/G/FRA) system PARSTAT 2273 (Princeton Applied Research Instruments, USA). The studies were performed in a buffer 0.1 M $(NH_4)_3BO_3$ + NH_4OH (pH 9.9) solution using a conventional three-electrode electrochemical cell. The solution was prepared from analytical grade reagents and deionized water (max. 0.1 μS/cm conductivity). Glass discs with deposited Mg-25Al-Zn thin films were used as working electrodes. The area of the working electrode surface exposed to electrolyte was 0.5 cm^2. Platinum plate of ~4 cm^2 area was used as a counter electrode and Ag/AgCl/ (saturated KCl solution) was used as a reference. EIS spectra were recorded under the open circuit potential in the potentiostatic mode with the potential amplitude of ±5 mV. The frequency range from 10 kHz to 0.1 Hz was employed, which permitted to perform a single scan in less than 1 min. Electrochemical measurements were initiated after 2.5–3 min of electrode exposure to the solution. This period was used to allow the sample to equilibrate with the surroundings before the scan was taken. EIS data analysis was performed using the authorized ZSimpWin™ software.

The mineral oil was coated on working electrodes by using wire wound drawdown bars (UVPS, Chicago, IL). The bars of the 0.25 mils size were used. The thickness of the applied film was adjusted to 5 μm (5.0 ± 0.4 μm) by gravimetric weighing before and after the coating on ALT100-5AM (Kern & Sohn GmbH, Germany) precision balance with accuracy of 10-microgram. It can be noted that thinner films could not be successfully coated on the electrode due to the film breakage and other non-homogeneities. The area of the oil-coated surface exposed to electrolyte was 0.5 cm^2.

RESULTS AND DISCUSSIONS

The main objective of the study was to establish a principal mechanism of formed Mg-based alloy corrosion in most typical applications and possible influence of a lubricant film on it. An inert ammonium borate electrolyte was selected, because it provides well-controlled halogenide-free media, more related to the corrosion conditions in the engine or hydraulic systems than NaCl electrolyte environment. The selected pH (9.9) value corresponded to the level of typical acid neutralizing additives used in most lubricant formula and, at the same, was more suitable to mitigate the high activity of Mg. On the other hand, widely used oil, namely paraffinic mineral oil, was chosen for studies due to its dominance in lubricant base stocks. Long-term corrosion performance of metals in great extent depends on the protective layer formed on its surface during initial steps of interaction with environment. Usually during this initial short-term period the most significant changes of surface properties take place. Passive film properties are highly dependent on the substrate microstructure and composition.

Electrochemical impedance spectroscopy (EIS) is a well-known technique for determining the electrical properties of ionic materials. The EIS permits characterization of charge and mass transport kinetics and charge-developing processes, which may take place both within the analyzed material and at the active interfaces of the system. Due to high precision and sensitivity, EIS has high experimental efficiency as it contains all necessary electrochemical information, which is needed to evaluate processes occurring in the system. The application of EIS technique for characterizing metal / oil / solution interfacial phenomena has been reported previously [27–31]. As known, the accuracy of parameters to be determined by EIS is highly dependent on the stability of the electrochemical system during measurements. The initial stages of corrosion are often characterized by fast changes of surface conditions. As a rather precise indicator of the stability of the electrochemical system open circuit electrode potential change (E_{ocp}) can be used. E_{ocp} variations of as-deposited (at 10 °C) and oil-coated Mg-25-Al-Zn electrodes in borate solutions are presented in Fig. 1. Apparently, for as-deposited Mg-25Al-Zn electrode the major changes of E_{ocp} occurred within the first ~2.5–3.0 min of exposure. For longer exposures the rate of E_{ocp} change did not exceed ~3–4 mV per ~15 min. For oil-coated electrodes a very similar trend of E_{ocp} change was also determined (curve 2). E_{ocp} values of oil-coated Mg-25Al-Zn electrodes were 30–60 mV more negative than those of uncoated ones. The shift of electrode potential towards the equilibrium potential of Mg oxidation indicates the ionic conductivity of oil film [31]. Both as-deposited and oil-coated electrodes demonstrated the E_{ocp} shifts in the direction of positive values in borate solutions. Such E_{ocp} tendency is a result of the passive oxide / hydroxide layer formation on the surface of Mg-25Al-Zn alloys. It could be mentioned that a similar character of E_{ocp} dependence on exposure times was also determined for Mg-25Al-Zn alloys deposited at 40, 80 and 150 °C. So, in order to reduce the error propagation due to electrode surface changes the first EIS scan was performed after ~3 min of immersion. The scan frequency range was chosen from 10 kHz to 0.1 Hz, reducing the total duration of one scan to less than 1 min.

Experimentally measured (symbols) and fitted (solid lines) impedance spectra of as-deposited and oil-coated Mg-25Al-Zn electrodes, deposited at 10, 40, 80 and 150 °C are presented in Fig. 2a, b in complex plane plot (or Nyquist)

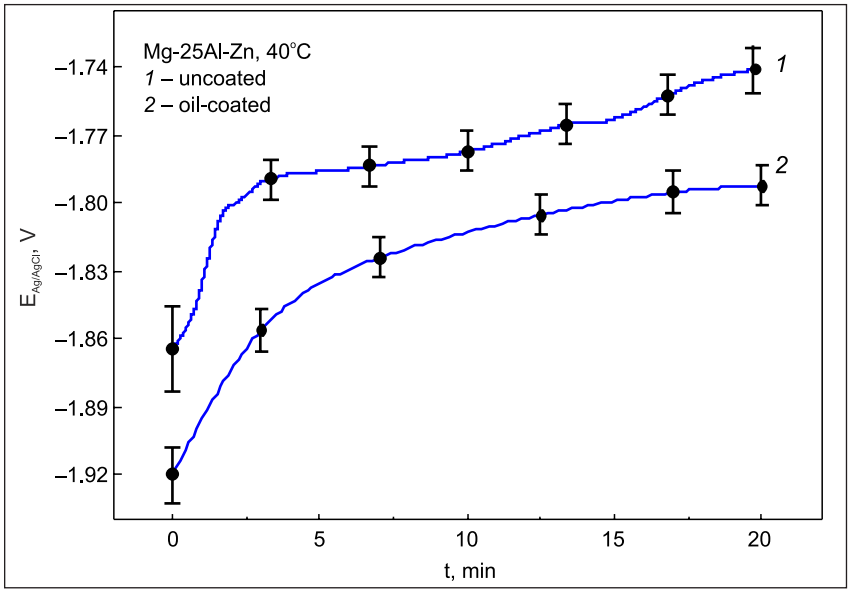

Fig. 1. E_{ocp} of magnetron-sputtered Mg-25Al-Zn alloys formed at 10 °C in ammonium borate solution: *1* – as-deposited, *2* – oil-coated

representation. Evidently, all spectra are characterized by well-defined semicircles (time constants) in the frequency range 10 kHz – 1 Hz and much less defined, distorted loops in the frequency range below approx. 1.0 Hz. Both real (Z_r) and imaginary (Z_{im}) impedance values of electrodes depend on alloy formation temperatures, i. e. the alloy's microstructure. The increase of alloy formation temperatures leads to larger coating's average grain sizes from ~12 to ~200 nm and the corresponding decrease of Z_r and Z_{im} components. In turn, a concurrent decrease of both Z_r and Z_{im} caused a significant reduction in polarization resistance (R_p) of the studied Mg-25Al-Zn electrode. R_p is the value that characterizes the corrosion resistance of electrodes and is defined as total electrode impedance at a constant current. For the most corrosion systems R_p can be estimated from EIS spectra by extrapolation of corresponding experimental or fitted impedance dependences to zero frequency. In the case of Nyquist representation, the Z_r value, intercepted by extrapolated line to zero frequency, must be corrected by subtracting the solution resistance (R_Ω). The largest decrease of R_p was determined for Mg-25Al-Zn alloy formed at 80 °C, which is characterized by the highest content of β-phase (Fig. 2a, curve 3). Most probably, that galvanic corrosion due to the formation of microcouples between the Mg matrix (α-phase) and β-phase additionally influenced the R_p value. As known, precipitation of the β phase is greatly affected by the alloy formation method, particularly by the temperature regime, and this component of alloy is

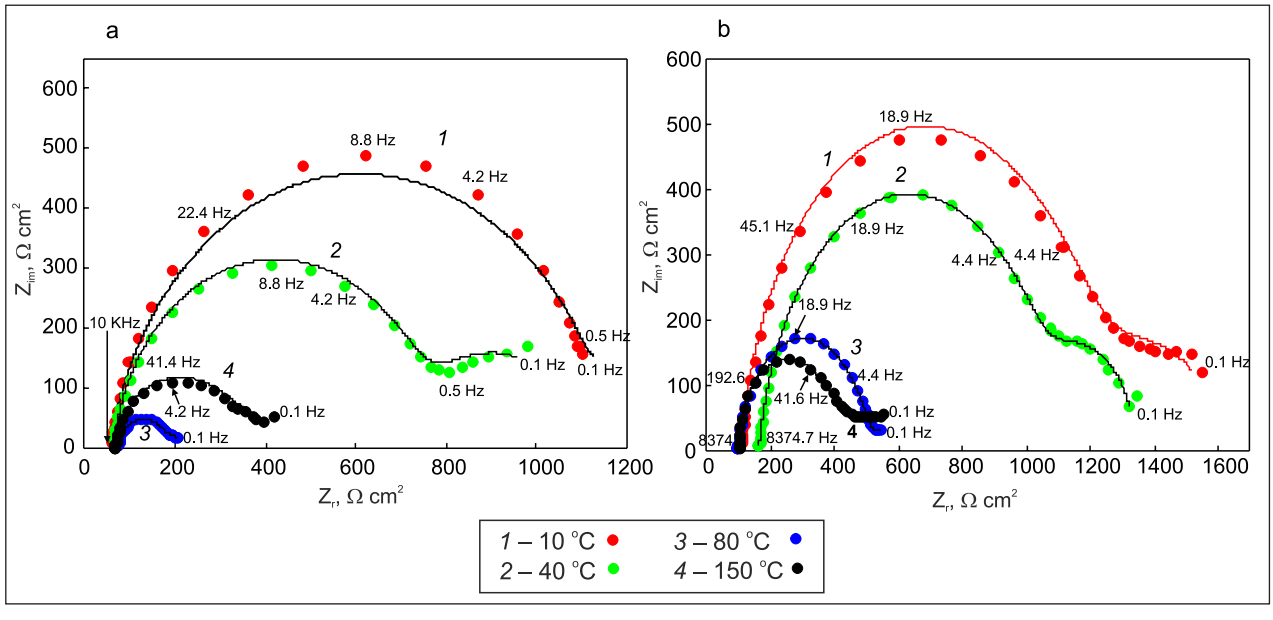

Fig. 2. Dependences of Nyquist plot on Mg-25Al-Zn alloy formation temperature: a – as-deposited, b – paraffin mineral oil-coated electrodes after 3 min of exposure in ammonium borate solution

predominantly localized alongside grain boundaries of the α-phase [32–36].

Several models of equivalent electrical circuit (EEC) were used for numerical simulation of electrode / electrolyte and electrode / oil / electrolyte interfaces. Voigt measurement models were regressed to the data for validation of experimental values and determination of the characteristic time constants that could be resolved for each scan [37]. For all studied electrodes in borate solutions a number of time constants were evaluated as 3. The tested alloy / electrolyte models are based on the phenomenon that oxide films, spontaneously formed in air and / or aqueous media, in great extent define the protective properties of metals. Such passive oxide films form a bilayer highly defective semiconductor structure, consisting of an inner (or barrier) layer adjacent to the metal and an outer one (or porous layer). The latter layer forms due to the reactions taking place between the metal and the outer medium. According to the point defect model (PDM), the barrier layer contributes most to the total impedance of the electrode whereas the resistance of the outer hydroxide porous layer is much lower [38–41]. Usually, in PDM the passive bilayer film is modelled by EEC consisting of two consecutively connected parallel (RC)-subcircuits in series with R_Ω: R – charge transfer resistance and C – double layer capacitance of the corresponding layer, R_Ω – resistance of the solution layer between the Luggin capillary tip and the working electrode. For pure Mg, which is characterized by a weak protective capability of the oxide / hydroxide layer, the EEC, which accounts for high porosity and permittivity, was proposed [42]. According to the proposed scheme, Mg dissolution occurs at the film-free areas and the Mg^{2+} ions, which are produced at the interface, diffuse through the inert porous Mg $(OH)_2$ layer. In the EEC, depicted in Fig. 3a, a resistance of the protective layer, consisting of Mg and Al oxides, was taken into account. In this model the electrolyte resistance across the oxide layer and the constant phase element (CPE) are represented by R_{ox} and CPE_{ox} elements, respectively; the parallel combination of R_{ct} and CPE_{ct} elements are attributed to the charge transfer (corrosion) process and the Warburg impedance element (W) represents diffusion limitations of the process [43, 44]. The coded formula of this EEC is recorded as $R_\Omega CPE_{ox} (R_{ox} (CPE_{ct}(R_{ct}W)))$. According to the used EEC scheme, reactions take place only at the end of the pore of the exposed electrode surface. Both R_{ox} and R_{ct} affect the corrosion process and their sum corresponds to the R_p value of the electrode. CPE parameter is usually introduced in EEC in order to get a better fit of a model with the real system response. This parameter was invented to take into account the surface roughness, inhomogeneity of coating's composition, reactivity, fractal geometry and possible diffusion limitations [44, 45]. The impedance of the CPE element Z_{CPE} is expressed by the equation:

$$Z_{CPE} = 1 / [Y_0 \times (j\omega)^n], \quad (1)$$

where Y_0 is the electrode admittance, j is the imaginary unit ($\sqrt{-1}$), $\omega = 2\pi f$ is the angular frequency of the exciting potential sine ($rad \cdot s^{-1}$), f is the frequency in Hz; the value of n ranges between 0 and 1. The values 0, 0.5 and 1 of n imply that CPE in the used EEC behaves as to be a pure resistor, Warburg impedance and capacitor, respectively. It can be mentioned that W as impedance originated due to diffusion processes and usually is observed in the low frequency range. As determined, the used EEC (Fig. 3a) provided the most satisfactory data fitting results for studied alloys, i. e. it was characterized by the lowest values of the "chi square" parameter (χ^2) and the weighted average error (as weighting factor impedance modulus was used). Attempts to add more components into EEC carried to unrealistically large errors for the new elements and significantly reduced the quality of fitting. The values of R_Ω were determined independently as being 2–5 $\Omega \cdot cm^2$ and were not fitted (were fixed at 2 $\Omega \cdot cm^2$). The fitted values of elements EEC are summarized in Table 1. Apparently, the used EEC fitted well with C_{ox} and C_{ct}. CPE elements were introduced only in some cases: for the alloy formed at 10 °C (as CPE_{ct}) and for alloys formed at 10 and 80 °C (as CPE_{ox}). In cases where the exponent n was close to 1, then CPE values were treated as capacitances. It can be noted that n should be >0.75 in order to have a reasonable confidence in C values [45]. Calculated C_{ct} and C_{ox} values are also listed in Table 1. The EIS data provide useful information regarding the nature of the coatings. For the alloy deposited at the lowest temperature (average grain

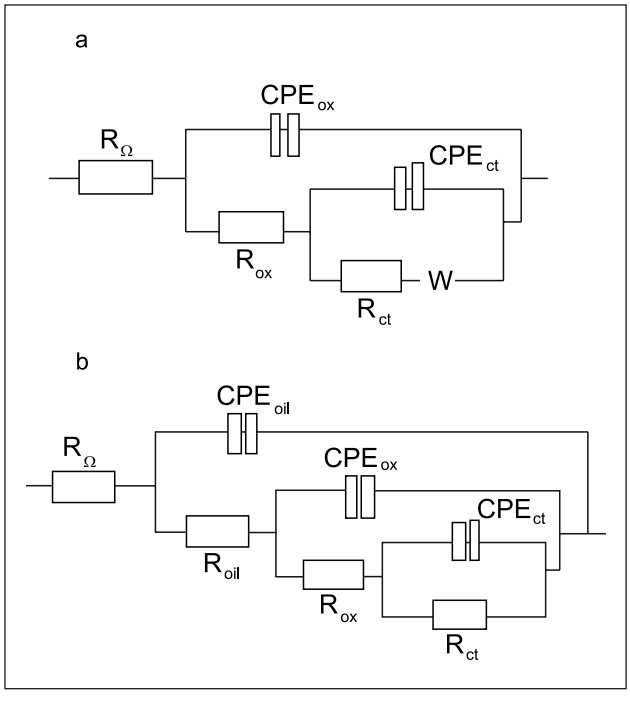

Fig. 3. Equivalent electrical circuits used for fitting of experimental EIS data: a – EEC for as-deposited Mg-25Al-Zn electrodes, b – EEC for oil-coated Mg-25-Al-Zn electrodes

Table 1. **Dependence of $R_\Omega(CPE_{ox}(R_{ox}(CPE_{ct}(R_{ct}W))))$ equivalent circuit parameters for as-deposited Mg-25Al-Zn electrodes formed at 10, 40, 80 and 150 °C in ammonium borate solution after 3 min of exposure**

T, °C	R_{ox}, Ω cm²	CPE_{ox}, $Ss^n cm^{-2}$; (n)	C_{ox}, F cm⁻²	R_{ct}, Ω cm²	CPE_{ct}, $Ss^n cm^{-2}$; (n)	C_{ct}, F · cm⁻²	W, $Ss^{0.5} cm^{-2}$	χ^2
10	754.0	$3.62 \cdot 10^{-5}$ (0.91)	$2.54 \cdot 10^{-5}$	344.2	0.00253 (0.86)	$2.5 \cdot 10^{-3}$	–	$9.96 \cdot 10^{-4}$
40	372.1	–	$1.8 \cdot 10^{-5}$	353.6	–	$2.2 \cdot 10^{-5}$	0.00414	$1.35 \cdot 10^{-3}$
80	167.2	$14.0 \cdot 10^{-5}$ (0.88)	$8.6 \cdot 10^{-5}$	38.5	–	$7.2 \cdot 10^{-3}$	0.0594	$9.5 \cdot 10^{-5}$
150	210.0	–	$10.1 \cdot 10^{-5}$	134.0	–	$38.3 \cdot 10^{-5}$	0.0182	$7.4 \cdot 10^{-4}$

size of coating ~12 nm) a value of charge transfer resistance R_{ct} = ~344.2 Ω · cm² and a considerably higher value of oxide layer resistance R_{ox} = ~754.0 Ω · cm² were obtained by fitting. It can be mentioned that the sum of R_{ct} and R_{ox} constitutes R_p. The increase of Mg-25Al-Zn formation temperatures to 40, 80 and 150 °C leads to a sharp decrease of R_{ox} to ~372.1, ~167.2 and ~210.0 Ω · cm², respectively. This general trend correlates well with the value of average grain size of corresponding coatings: ~50, ~120 and ~200 nm. The lowest value of R_{ct} for the alloy deposited at 80 °C must be noted. Such a deviation of tendency, i. e. the lowest values of R_{ox} = ~167.2 Ω · cm² and R_{ct} = ~38.5 Ω · cm² for the alloy formed at 80 °C, certainly correlates with the highest content of β-phase in coating and, respectively, high contribution of microgalvanic corrosion. The influence of the coating microstructure on C_{ct} and W is also evident; however, a proven tendency was not established. Nevertheless, it could be mentioned that for Mg-25Al-Zn alloys formed at higher temperatures, especially for the one formed at 80 °C, the influence of β-phase on initial stages of corrosion is very substantial. According to the fitted C_{ox} values (Table 1), the thickness of the protective layer (*d*) was estimated from the relationship:

$$d = \varepsilon\varepsilon_0 S/C, \tag{2}$$

where S = 0.5 cm² is the area of used electrode, $\varepsilon_0 = 8.85 \times 10^{-14}$ F · cm⁻¹ is the vacuum permittivity [46]. Assuming ε ~10, which is a relative dielectric constant of mixed magnesium-aluminium oxide, the thickness of the oxide layer for alloys formed at 10, 40, 80 and 150 °C was estimated as ~17.5, ~20, ~5 and ~4.5 nm, respectively. An attempt to separate the contributions of "barrier" and "porous" components of the oxide layer into R_{ox} and C_{ox} led to the unrealistically high increase of fitted R_{ct} (~10^6–10^7 Ω · cm²) and unduly large errors (the relative standard errors were >1 000%). So, the analysis of EIS data clearly shows the dependence of the corrosion resistance of Mg-25Al-Zn alloy on its microstructure: corrosion resistance increased with smaller grain sizes, the thicker oxide / hydroxide layers and lower contents of the β-phase in alloys.

As known, oil films effectively retard metals corrosion [27–31]. The layer of oil acts as a barrier between metal and corrosion medium. The protective ability of such layer is determined by lower electronic conductivity in comparison with that of electronic conductors. So, the metal covered by oil may be qualified as a specific metal / oil / electrolyte electrochemical system where anodic and cathodic reactions occur simultaneously at metal / oil and oil / electrolyte interfaces, respectively. It is highly probable that in electrolytes the oil conductivity might change due to the ion uptake into the oil film. In turn, those processes would have an influence on metal corrosion.

Measured (symbols) and fitted (solid lines) impedance spectra of oil-coated Mg-25Al-Zn electrodes are presented in Fig. 2b. The spectra are characterized by single well-defined capacitive semicircles in the frequency range from ~10 kHz to ~1 Hz, followed by a distorted part of spectrum in the frequency range below approx. 1.0 Hz. Apparently, the impedance values of oil-coated electrodes are higher than those of oil-free electrodes. The impedance of electrodes also depended on alloy formation temperatures as in the case of oil-free electrodes. So, the increase of the alloy formation temperature that corresponded to the increase in average grain sizes of the coating led to the decrease of the corresponding electrode impedance in the order 10, 40, 80 and 150 °C. However, contrary to oil-free electrodes for oil-coated ones there was no evidence that the β-phase had much influence: i. e., the position of impedance dependence of the Mg-25Al-Zn alloy, characterized by the biggest content of the β-phase (formed at 80 °C), corresponded to the temperature increase sequence (Fig. 2a, b, curve 3). So, it may be proposed that paraffin oil inhibited the "microgalvanic" effect of the β-phase.

Evaluation of impedance spectra of oil-coated electrodes by the Voigt measurement model [37] showed that the number of time constants that could be reliably resolved for each scan was three. The model of two superimposed porous layers was used for modelling of the electrode / oil / electrolyte interface. This model is commonly used to describe corrosion of metals under organic protective layers, electrochemical behaviour of polyaniline-modified electrodes and oil-coated ones, etc. [28, 30, 47, 48]. An arrangement of this EEC, which coded formula is written as $R_\Omega(C_{oil}(R_{oil}(CPE_{ox}(R_{ox}(CPE_{ct}R_{ct})))))$, is presented in Fig. 3b. The used EEC scheme can be considered as modification of EEC used for oil-uncoated electrodes (Fig. 3a), which is supplemented by an additional ($R_{oil}C_{oil}$) sub-circuit. The inserted ($R_{oil}C_{oil}$) sub-circuit represents an additional oil / electrolyte interface, where R_{oil} is the electrolyte resistance across oil pores, C_{oil} is the capacitance of an oil layer. In this study the ~5 μm thickness oil films were coated on electrodes with a ~1 μm thick magnetron-sputtered Mg-25Al-Zn layer. As known, the dielectric constant value ε = 3–8 is characteristic for the most liquid organic compounds. According

to the relationship (2), the capacitance of 5.0 ± 0.4 μm oil film should be approximately (0.5–1.54) × 10^{-9} F · cm^{-2}. An electrical conductivity of oils highly depends on the contents of water and polar additives and impurities. Clean, dry base oils (highly treated ones containing minimum amounts of impurities and polar components) have a very low conductivity ~(10^{-14}–10^{-13}) S · cm^{-1} [49]. The presence of oil-based colloidal additives, such as alkylsalicylates, sulfonates or other, increases the conductivity to (10^{-8}–10^{-5}) S · cm^{-1} or higher. Thus, wet, impure or used oils may act as electrolytes. In our study, the resistance of the ~5.0 μm thickness oil film, whose conductivity is in the range ~(10^{-6}–10^{-5}) S · cm^{-1}, would be ~(25–250) Ω · cm^2. The corresponding range of characteristic frequencies for this oil film would be ~(2.5–80.0) × 10^6 Hz. It is evident that these values of frequencies are above possible range of the used EIS instrument and the capacitive loops corresponding to such layer were not observed in experimental spectra. Nonetheless, the resistance of the oil layer definitely affects experimental impedance spectra at all frequencies, which can be seen from the increase of R_Ω in the frequency range 10^3–10^4 Hz (Fig. 2b). Due to the above mentioned reasons the fitting of the "high-frequency" ($R_{oil}C_{oil}$) circuit from impedance data measured in medium- and low-frequency ranges would not be precise.

The results of the experimental spectra fitting of oil-coated Mg-25Al-Zn electrodes are presented in Table 2. The magnitude of R_Ω = 2 Ω was fixed as in the case of oil-free electrodes. The influence of "pure" diffusion (W impedance) for all oil-coated electrodes was determined as insignificant and this element was excluded from EEC. At the same time, it should be noted that for the ($R_{ct}CPE_{ct}$) sub-circuit the values of n < 0.75 were fitted. Therefore, the CPE_{ct} parameter could not be treated as a capacitor. Most likely, the influence of diffusion superimposed with effects of such factors as surface roughness, inhomogeneity and so on. The calculated values of R_{oil} of the "high-frequency" ($R_{oil}C_{oil}$) circuit were as follows: ~113.2 Ω · cm^2 for Mg-25Al-Zn alloy formed at 10 °C and ~127.5, ~103.7, ~110.5 Ω · cm^2 for alloys formed at 40, 80, and 150 °C, respectively. It should be mentioned that these R_{oil} values were of the same order as calculated: ~25–250 Ω · cm^2. The fitted C_{oil} values of the oil film for the same temperature sequence were ~3.05 × 10^{-6}, ~1.02 × 10^{-6}, ~4.43 × 10^{-6} and ~0.12 × 10^{-6} F · cm^{-2}, respectively. These values were considerably higher than calculated ones according to the equation (2) and could not be regarded as strictly correct. As mentioned, corresponding capacitive loops were not observed in experimental spectra and an impact of the ($R_{oil}C_{oil}$) sub-circuit resulted only in changes of the oil layer resistance R_{oil}.

Although some correlation between changes of the R_{oil} and C_{oil} parameters and the alloy microstructure can be discerned, it is hardly credible that the substrate (alloy) could affect the oil layer. Meanwhile, a more reasonable correlation between the coating microstructure and parameters of the hydroxide layer along with those of charge transfer reaction were determined. As shown in Table 2, the Mg-25Al-Zn alloys with smaller size of crystallites are characterized by larger values of R_{ox}, i. e. are more corrosively resistant. Thus, for the alloy formed at 10 °C the fitted R_{oxt} was ~1 107 Ω · cm^2, for alloys formed at 40, 80, and 150 °C R_{ox} were ~916.3, ~392.1 and ~334.3 Ω · cm^2, respectively. The sharp decrease of R_{ox} for alloys formed at temperatures above 40 °C, obviously, could be attributed to the additional detrimental influence of the β-phase, the content of which in this alloy was the highest. The impact of the β-phase could be explained by acceleration of the cathodic reaction of the corrosion process due to more positive values of E_{corr} of intermetallic $Mg_{17}Al_{12}$ compound, i. e. by formation of the α-phase / β-phase galvanic couple. The dependence of fitted C_{ox} values on the alloy formation temperature confirmed that thinner oxide films (higher values of C_{ox}) formed on larger crystallites. At the same time, the correlation between parameters of the charge transfer reaction (i. e. the R_{ct} and CPE_{ct}) and the coating structure was not evident. Thus, rather similar values of the charge transfer resistance R_{ct} were calculated for all studied Mg-25Al-Zn alloys formed at different temperatures. At the same time, the fitted CPE_{ct} values differed considerably and it was not possible to find any reasonable correlation with the coating grain size or β-phase content. It is obvious that additional studies are needed to differentiate the concurrent effects of surface roughness, inhomogeneity, diffusion etc. from charge transfer factors.

The evolution of Nyquist impedance spectra of oil-free and oil-coated Mg-25Al-Zn electrodes immersed in borate solutions on exposure time is shown in Fig. 4a, b. Measurements were carried out after 3, 10 and 20 min of exposure under open circuit conditions. These alloys were deposited at 10 °C and, hence, did not have β-phase that influenced the corrosion process. Evidently, in both cases the real and imaginary parts of impedance increased during the exposure. This also translated into the increase of the polarization resistance of electrodes R_p and, respectively, the decrease of the alloy corrosion rate. The measured spectra were fitted by the same EECs (Fig. 3) without including any

Table 2. **Dependence of $R_\Omega(C_{oil}(R_{oil}(CPE_{ox}(R_{ox}(CPE_{ct}R_{ct}))))$ equivalent circuit parameters for paraffin mineral oil-coated Mg-25Al-Zn electrodes formed at 10, 40, 80 and 150 °C in ammonium borate solution after 3 min of exposure**

T, °C	R_{oil}, Ω cm^2	C_{oil}, F cm^{-2}	R_{ox}, Ω cm^2	CPE_{ox}, Ss^n cm^{-2}; (n)	C_{ox}, F cm^{-2}	R_{ct}, Ω cm^2	CPE_{ct}, Ss^n cm^{-2}; (n)	χ^2
10	113.2	3.05 · 10^{-6}	1 107	1.1 · 10^{-5} (0.99)	5.6 · 10^{-6}	398.1	0.00172 (0.71)	3.9 · 10^{-4}
40	127.5	1.02 · 10^{-6}	916.3	2.05 · 10^{-5} (0.89)	12.8 · 10^{-6}	365.5	0.002 (0.693)	6.54 · 10^{-5}
80	103.7	4.43 · 10^{-6}	392.1	3.56 · 10^{-5} (0.88)	19.9 · 10^{-6}	367.9	0.018 (0.38)	1.85 · 10^{-4}
150	110.5	0.12 · 10^{-6}	334.2	1.43 · 10^{-5} (0.88)	6.9 · 10^{-6}	374.3	0.0056 (0.48)	5.18 · 10^{-4}

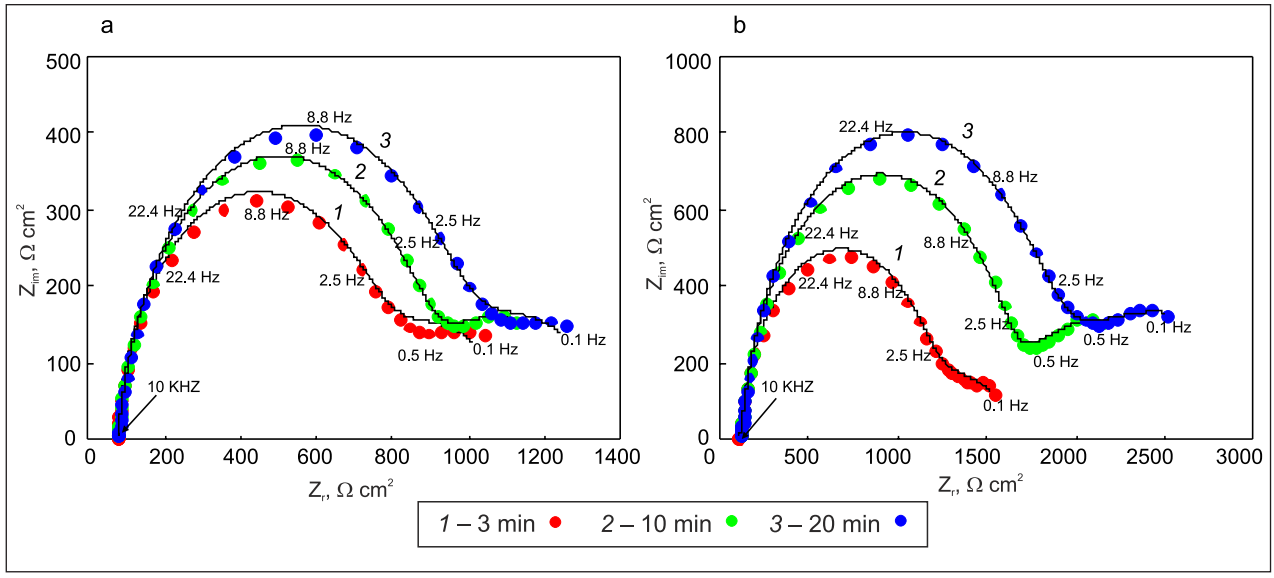

Fig. 4. Evolution of Nyquist plots of as-deposited (a) and paraffin mineral oil-coated (b) Mg-25Al-Zn electrodes formed at 10 °C on exposure time in ammonium borate solution

additional elements in the schemes. It can be noted that for all spectra the quality of fitting was not worse than before. The fitted parameters of EECs are presented in Tables 3 and 4. For the oil-free Mg-25Al-Zn electrodes the increase of R_{ox} from ~754.0 Ω · cm^2 (fitted value corresponded to 3 min of exposure) to ~866.2 Ω · cm^2 and ~967.9 Ω · cm^2 after 10 and 20 min, respectively, was determined. The increase of R_{ox} suggested an increase of electrode corrosion resistance. At the same time, the decrease of corresponding values of C_{ox} from ~2.54×10^{-5} to ~1.71×10^{-5} F · cm^{-2} denoted the thinning of the protective oxide / hydroxide layer. According to the relationship (2) the thickness of the oxide layer decreased from ~17.5 to ~11.8 nm. The most probable cause of such opposite trends is an enrichment of the developed oxide layer with Al oxide, which is more compact and has a considerably higher protective capability than Mg oxide. The increase (enrichment) of the protective oxide layer developed on Al-Mg and Mg-Cr alloys during exposure in corrosion environment by a nobler component (Al or Cr, respectively) was shown in our previous works [50–52]. It can be mentioned that this well-known phenomenon is often observed for stainless steels: for instance, it was determined for magnetron-sputtered Fe-Cr-Ni alloys with additives of Ta [53]. As for charge transfer parameters, a relatively minor increase of R_{ct} from ~344.2 Ω · cm^2 at 3 min of exposure to ~390.1 Ω · cm^2 and ~385.5 Ω · cm^2 after 10 and 20 min of exposure, respectively, was determined. The fitted values of C_{ct} were the same at all exposure times. It could be noted that such stability of EEC parameters corresponded well with above slow changes of E_{ocp} (~3–4 mV per ~15 min) at the same exposure times (Fig. 1).

Similar tendencies for oxide layer parameters were also found in case of oil-coated Mg-25Al-Zn electrodes (Table 4). It is obvious that the increase in R_{ox} and the decrease of C_{ox} during exposure were caused by the same reasons as for oil-free electrodes. At the same time, a considerable increase of R_{ct} during exposure requires a special analysis. It is highly probable that a detailed investigation of causes, which determine the character of CPE_{ct}, will lead to the interpretations similar to those of oil-free electrodes.

Table 3. **Dependence of $R_\Omega(CPE_{ox}(R_{ox}(CPE_{ct}R_{ct})))$ equivalent circuit parameters for as-deposited Mg-245Al-Zn electrodes deposited at 10 °C on exposure time**

t, min	R_{ox}, Ω cm^2	CPE_{ox}, Ss^n cm^{-2}; (n)	C_{ox}, F cm^{-2}	R_{ct}, Ω cm^2	CPE_{ct}, Ss^n cm^{-2}; (n)	C_{ct}, F cm^{-2}	χ^2
3	754.0	$3.62 \cdot 10^{-5}$ (0.91)	$2.54 \cdot 10^{-5}$	344.2	0.0025 (0.86)	0.0024	$9.86 \cdot 10^{-4}$
10	866.2	$2.74 \cdot 10^{-5}$ (0.90)	$1.81 \cdot 10^{-5}$	390.1	0.00298 (0.87)	0.0028	$6.32 \cdot 10^{-4}$
20	967.9	$2.58 \cdot 10^{-5}$ (0.90)	$1.71 \cdot 10^{-5}$	385.5	0.0025 (0.84)	0.00248	$5.83 \cdot 10^{-4}$

Table 4. **Dependence of $R_\Omega(C_{oil}(R_{oil}(CPE_{ox}(R_{ox}(CPE_{ct}R_{ct}))))$ equivalent circuit parameters for paraffin mineral oil-coated Mg-245Al-Zn electrodes deposited at 10 °C on exposition time**

t, min	R_{oil}, Ω cm^2	C_{oil}, F cm^{-2}	R_{ox}, Ω cm^2	CPE_{ox}, Ss^n cm^{-2}; (n)	C_{ox}, F cm^{-2}	R_{ct}, Ω cm^2	CPE_{ct}, Ss^n cm^{-2}; (n)	χ^2
3	103.2	$3.05 \cdot 10^{-6}$	1 107	$1.1 \cdot 10^{-5}$ (0.99)	$5.6 \cdot 10^{-6}$	398.1	0.00172 (0.71)	$3.9 \cdot 10^{-4}$
10	101.7	$1.1 \cdot 10^{-6}$	1 608	$8.8 \cdot 10^{-6}$ (0.9)	$5.5 \cdot 10^{-6}$	750.3	0.00153 (0.84)	$2.94 \cdot 10^{-4}$
20	104.8	$1.07 \cdot 10^{-6}$	1 799	$1.26 \cdot 10^{-6}$ (0.9)	$0.64 \cdot 10^{-6}$	1 113	0.00112 (0.65)	$4.47 \cdot 10^{-5}$

CONCLUSIONS

The short-term corrosion behaviour of as-deposited and paraffin oil-coated Mg-25Al-Zn alloys, formed by the direct current magnetron-sputtering technique, was studied in buffer ammonium borate solutions by the EIS method. On the basis of experimental EIS results and process modelling, the following conclusions were made.

1. The coating microstructure and resistance of the oxide layer spontaneously developed at the coating / solution interface considerably influenced short-term corrosion of Mg-25Al-Zn alloys. Magnetron sputtered Mg-25Al-Zn coatings characterized by the finest grain size and lower content of β-phase were more corrosion resistant at studied exposure times. The initial thickness of the oxide layer depended on the Mg-25Al-Zn alloy formation temperature: it varied from ~5 nm at 10 and 40 °C to ~15–20 nm at 150 °C.

2. The thickness of the surface oxide layer decreased during exposure in ammonium borate solution. A simultaneous increase of the total electrode impedance and, respectively, corrosion resistance of the coating, was attributed to enrichment of the oxide layer with aluminium oxide.

3. Very similar tendencies of corrosion behaviour for Mg-25Al-Zn alloys coated with a ~5 μm film of paraffin mineral oil were determined on the basis of EIS data analysis and modelling. At the same time, it could be noted that paraffin mineral oil suppressed the impact of β-phase.

Presented data can be useful for development of more corrosion-resistant Mg alloys and selection of suitable lubricants and rust protection materials.

ACKNOWLEDGEMENTS

The authors express their gratitude to Dr. A. Selskis for SEM, Dr. Juškėnas for XRD and Dr. A. Suchodolskis for AFM measurements of Mg-25Al-Zn alloys.

Received 9 October 2012
Accepted 9 November 2012

References

1. K. Funatani, *Surf. Coat. Technol.*, **133–134**, 264 (2000).
2. G. Song, A. Atrens, X. Wu, B. Zhang, *Corros. Sci.*, **39(10)**, 1769 (1998).
3. M. Bamberger, G. Dehm, *Annu. Rev. Mater. Res.*, **38**, 505 (2008).
4. L. J. Liu, M. Schlesinger, *Corros. Sci.*, **51**, 1733 (2009).
5. M. Regev, O. Botstein, M. Bamberger, A. Rosen, *Mater. Sci. Eng., A*, **302**, 51 (2001).
6. J. E. Gray, B. Luan, *J. Alloys Compd.*, **336**, 88 (2002).
7. M. P. Staiger, A. M. Pietak, J. Huadmai, G. Dias, *Biomaterials*, **27**, 1728 (2006).
8. F. Witte, *Acta Biomater.*, **6**, 1680 (2010).
9. M. Alvarez-Lopez, M. D. Pereda, J. A. del Valle, et al., *Acta Biomater.*, **6**, 1763 (2010).
10. C. Blawert, D. Manova, M. Störmer, J. W. Gerlach, W. Dietzel, S. Mändl, *Surf. Coat. Technol.*, **202**, 2236 (2008).
11. A. Grigucevičienė, K. Leinartas, R. Juškėnas, E. Juzeliūnas, *J. Electroanal. Chem.*, **565**, 203 (2004).
12. E. Juzeliūnas, A. Grigucevičienė, K. Leinartas, R. Juškėnas, *Electrochem. Commun.*, **6**, 678 (2004).
13. A. Grigucevičienė, K. Leinartas, R. Juškėnas, E. Juzeliūnas, *Mater. Sci. Eng., A*, **394**, 411 (2005).
14. H. Gleiter, *Acta Mater.*, **48**, 1 (2000).
15. K. S. Kumar, H. van Swygenhoven, S. Suresh, *Acta Mater.*, **51**, 5743 (2003).
16. M. Bamberger, *Mater. Sci. Technol.*, **1**, 15 (2001).
17. S. F. Liu, L. Y. Liu, L. G. Kang, *J. Alloys Compd.*, **450**, 546 (2008).
18. S. Mathieu, C. Rapin, J. Steinmetz, P. Steinmetz, *Corros. Sci.*, **45**, 2741 (2003).
19. A. Eliezer, O. Medlinsky, J. Haddad, G. Ben-Hamu, *Mater. Sci. Eng., A*, **477**, 129 (2008).
20. R. M. Mortier, S. T. Orszulik, *Chemistry and Technology of Lubricants*, Blackie Academic & Professional, London (1992).
21. S. Q. A. Rizvi, *Lubricants and Lubricant Additives*, Lubrizol Corp. (1995).
22. H. Wagner, T. Mang, R. Luther, *Appl. Catal., A*, **221**, 429 (2001).
23. G. Biresaw, A. Adhvaryu, S. Z. Erhan, C. J. Carriere, *J. Am. Oil Chem. Soc.*, **79**, 53 (2002).
24. M-Ch. Zhao, M. Liu, G. Song, A. Atrens, *Corr. Sci.*, **50**, 1939 (2008).
25. Y. Song, E.-H. Han, D. Shan, Ch. D. Yim, B. S. You, *Corr. Sci.*, **60**, 238 (2012).
26. A. Grigucevičienė, D. Bražinskienė, K. Leinartas, P. Miečinskas, S. Asadauskas, *Proceedings of International Conference on Functional Nanocoatings*, Dresden, Germany (2010).
27. M. F. Smiechowski, V. F. Lvovich, *J. Electroanal. Chem.*, **534**, 171 (2002).
28. V. F. Lvovich, M. F. Smiechowski, *Electrochim. Acta*, **51**, 1487 (2006).
29. V. F. Lvovich, M. F. Smechowski, *Electrochim. Acta*, **53**, 7375 (2008).
30. K. N. Allahar, D. P. Butt, M. E. Orazem, et al., *Electrochim. Acta*, **51**, 1497 (2006).
31. Q. D. Zhong, M. Rohwerder, Z. Zhao, Z. Jin, *J. Electrochem. Soc.*, **151(7)**, B446 (2004).
32. C. Suman, *SAE Trans.*, **99(5)**, 849 (1990).
33. G. Song, A. Atrens, X. Wu, Bo Zhang, *Corros. Sci.*, **40(10)**, 1769 (1998).
34. G. Song, A. Atrens, M. Dargusch, *Corros. Sci.*, **41**, 249 (1999).
35. Zh. Shi, G. Song, A. Atrens, *Corros. Sci.*, **47**, 2760 (2005).
36. M-C. Zhao, M. Liu, G. Song, A. Atrens, *Corros. Sci.*, **50**, 1939 (2008).
37. P. Agarwal, M. E. Orazem, L. H. Garcia-Rubio, *J. Electrochem. Soc.*, **139**, 1917 (1992).
38. D. D. Macdonald, *J. Electrochem. Soc.*, **139**, 3434 (1992).
39. D. D. Macdonald, A. Sun, N. Priyantha, P. Jayaweera, *J. Electroanal. Chem.*, **572**, 421 (2004).

40. J. Ai, Y. Chen, M. Urquidi-Macdonald, D. D. Macdonald, *J. Electrochem. Soc*., **154**, C43 (2007).
41. J. Ai, Y. Chen, M. Urquidi-Macdonald, D. D. Macdonald, *J. Electrochem. Soc*., **154**, C52 (2007).
42. G. Baril, G. Galicia, C. Deslouis, N. Pébère, B. Tribollet, V. Vivier, *J. Electrochem. Soc.*, **154(2)**, C108 (2007).
43. L. Bousselmi, C. Fiaud, B. Tribollet, E. Triki, *Electrochim. Acta*, **44**, 4357 (1999).
44. M. Orazem, B. Tribollet, *Electrochemical Impedance Spectroscopy*, John Wiley & Sons, Inc., Hoboken, NJ (2008).
45. C. S. Hsu, F. Mansfeld, *Corrosion*, **57(9)**, 747 (2001).
46. *Relative Dielectrics Constant* ε_r *(dk Value) of Liquids and Solid Materials* [http://www.de.endress.com].
47. C. I. Elsner, E. Cavalcanti, O. Ferraz, A. R. Di Sarli, *Prog. Org. Coat.*, **48**, 50 (2003).
48. L. Fedrizzi, F. J. Rodriguez, S. Rossi, F. Deflorian, R. Di Maggio, *Electrochim. Acta*, **46**, 3715 (2001).
49. L. A. Bronshtein, Yu. N. Shekhter, V. M. Shkolnikov, *Chem. Tech. Fuels Oil+*, **15(5)**, 350 (1979).
50. V. Uksienė, K. Leinartas, R. Juškėnas, A. Sudavičius, E. Juzeliūnas, *Electrochem. Commun.*, **4**, 747 (2002).
51. E. Juzeliūnas, K. Leinartas, W. Furbeth, K. Juttner, *Corros. Sci.*, **45**, 1939 (2003).
52. M. Samulevičienė, P. Miečinskas, K. Leinartas, et al., *Mater. Chem. Phys.*, **126**, 898 (2011).
53. K. Leinartas, M. Samulevičienė, A. Bagdonas, R. Juškėnas, E. Juzeliūnas, *Surf. Coat. Technol.*, **168**, 70 (2003).

L. Staišiūnas, A. Grigucevičienė, P. Miečinskas, D. Bražinskienė, S. J. Asadauskas, K. Leinartas

PLONASLUOKSNIŲ MAGNETRONINIŲ MG-25AL-ZN LYDINIO DANGŲ PRADINIŲ KOROZIJOS STADIJŲ TYRIMAI ELEKTROCHEMINIO IMPEDANSO SPEKTROSKOPIJOS METODU AMONIO BORATINIAME TIRPALE

S a n t r a u k a

Apie 1 μm storio Mg-25Al-Zn lydinio (at.%: Al – ~25, Zn – 0,5–1,0 ir Mg – likusi dalis) sluoksniai buvo suformuoti ant stiklo padėklų pastovios srovės magnetroninio dulkinimo metodu. Elektrocheminio impedanso spektroskopijos (EIS) metodas buvo naudojamas tirti pradinėms Mg-25Al-Zn lydinio korozijos stadijoms amonio boratiniame tirpale. Nustatyta, kad lydinio koroziją veikia jo mikrostruktūra (fazinė sudėtis, kristalitų dydis) ir oksidinio sluoksnio, savaime susidarančio tarpfaziu elektrodas / elektrolitas, storis ir elektrinė varža. Lydiniai, charakterizuojami mažesniais kristalitų dydžiais ir mažesniu β-fazės kiekiu, buvo labiau atsparūs korozijai. Pradinis oksidinio sluoksnio storis priklauso nuo lydinio formavimo temperatūros: jis keičiasi nuo ~5 nm esant 10 °C iki ~15–20 nm esant 150 °C. EIS metodu taip pat buvo tiriama Mg-25Al-Zn lydinio, padengto mineraline alyva, korozija. Nustatyta, kad nepadengtų Mg-25Al-Zn lydinių ir padengtų ~5 μm storio sluoksnio alyva korozijos mechanizmai yra panašūs. Ekspozicijos tirpale oksidinio sluoksnio storis mažėja. Mineraline alyva padengtuose bandiniuose slopinamas β-fazės poveikis. Nustatytas elektrodo korozinio atsparumo didėjimas yra aiškinamas paviršinio sluoksnio praturtinimu aliuminio oksidu.